Tumor cell nuclei soften during transendothelial migration

Anya B. Roberts[1], Jitao Zhang[2], Vijay Raj Singh[3,4], Miloš Nikolić[5], Emad Moeendarbary[6], Roger D. Kamm[†,1,3], Peter T. C. So[‡,1,3,4], Giuliano Scarcelli[*2,5]

[1]*Department of Biological Engineering, Massachusetts Institute of Technology, Cambridge, 02139, MA*

[2]*Fischell Department of Bioengineering, University of Maryland, College Park, 20742, MD*

[3]*Department of Mechanical Engineering, Massachusetts Institute of Technology, Cambridge, 02139, MA*

[4]*Laser Biomedical Research Center, Massachusetts Institute of Technology, Cambridge, 02139, MA*

[5]*Maryland Biophysics Program, University of Maryland, College Park, MD 20742, USA.*

[6] Department of Mechanical Engineering, University College London, London WC1E 7JE, UK

[†]*rdkamm@mit.edu,* [‡]*ptso@mit.edu,*[*] *sarc@umd.edu*

During cancer metastasis, tumor cells undergo significant deformation in order to traverse through endothelial cell junctions in the walls of blood vessels. As cells pass through narrow gaps, smaller than the nuclear diameter, the spatial configuration of chromatin must change along with the distribution of nuclear enzymes. Nuclear stiffness is an important determinant of the ability of cells to undergo transendothelial migration, yet no studies have been conducted to assess whether tumor cell cytoskeletal or nuclear stiffness changes during this critical process in order to facilitate passage. To address this question, we employed two non-contact methods, Brillouin confocal microscopy (BCM) and confocal reflectance quantitative phase microscopy (QPM), to track the changes in mechanical properties of live, transmigrating tumor cells in an *in vitro* collagen gel platform. Using these two imaging modalities to study transmigrating MDA-MB-231, A549, and A375 cells, we found that both the cells and their nuclei soften upon extravasation and that the nuclear membranes remain soft for at least 24 hours. These new data suggest that tumor cells adjust their mechanical properties in order to facilitate extravasation.

Original Article for submission to the Journal of Biomechanics for the Biofluids Symposium special issue
Keywords: Brillouin microscopy, Interference microscopy, Metastasis, Cell modulus

1. Introduction

The mechanical properties of a tumor cell and its nucleus play a critical role in cancer metastasis, especially since tumor cells transit through diverse microenvironments (Denais and Lammerding, 2014; Friedl et al., 2011). During metastatic transendothelial migration (TEM), tumor cells extend protrusions through what are likely to be spontaneously-formed endothelial gaps in the blood vessel wall (Escribano et al., 2019). As these leading protrusions penetrate the endothelium, $\beta 1$ integrin activation facilitates adhesion to the basement membrane laminin in the subendothelial extracellular matrix (ECM) (Chen et al., 2016). To complete the process of TEM, the cell utilizes actomyosin contraction to pull the rest of itself through the endothelial gap (Kale et al., 2015; Reymond et al., 2015). During TEM, tumor cells deform to sizes smaller than the initial nucleus, the stiffest and largest organelle in the cell. Since the nucleus is 3-10x stiffer than the cytoplasm (Caille et al., 2002; Guilak et al., 2000), these deformations are thought to be a limiting factor in TEM, as demonstrated in vitro (Chen et al., 2017) and previously modeled theoretically (Cao et al., 2016).

Previous *in vitro* work has revealed that cellular and nuclear stiffness are key factors in cancer metastasis. Tumor cells of greater metastatic potential are known to be softer (Cross et al., 2007; Guck et al., 2005; Han et al., 2020; Swaminathan et al., 2011). Additionally, nuclear softening by lamin A/C reduction facilitates cell migration through pores in ECM-like matrices and tight engineered constrictions comparable in size to gaps between endothelial cells during TEM (Davidson et al., 2014; Davidson et al., 2015; Harada et al., 2014; Ribeiro et al., 2014; Rowat et al., 2013; Wolf et al., 2013). Similarly, a softer nucleus may better facilitate migration through endothelial cell junctions. However, too soft of a nucleus could also leave a tumor cell vulnerable to nuclear membrane rupture and DNA damage (Denais et al., 2016; Harada et al., 2014), either

during TEM or under the shear stresses of circulation preceding it. While previous studies have focused on observing nuclear deformation through fixed constrictions, no published studies have examined whether nuclear stiffness dynamically changes during transendothelial migration to facilitate this process and whether these changes persist.

Measurements of the Young's modulus of the nucleus vary widely from 0.1-10 kPa, depending on the technique and cell type (Caille et al., 2002; Dahl et al., 2005; Deguchi et al., 2005; Deguchi et al., 2007; Guilak et al., 2000; Liu et al., 2014; Tseng et al., 2004). In part, this variability stems from the difficulty of measuring nuclear stiffness in its intact state and environment, and that most measurements (such as micropipette aspiration, compression via parallel plates, optical tweezers, cantilever tensile test, and atomic force microscopy) require isolation of the nucleus from the cell in a potentially destructive process. Moreover, all these methods require direct physical perturbation of the nucleus which may alter the mechanical properties of the nucleus since the nucleus and surrounding cytoplasm are mechanically connected (Lombardi et al., 2011) and cells can react to external stimulus. Particle tracking microrheology can examine intracellular and plasma membrane forces (Herráez-Aguilar et al., 2020; Wirtz, 2009; Yamada et al., 2000); however, this approach involves invasive delivery of particles into the cells and isolation of the nucleus in some cases. In general, methods to assess intracellular mechanics are highly perturbative and would not be possible while a cell is undergoing TEM. In order to make meaningful measurements of stiffness during and after TEM, it is therefore preferable to use a method that does not affect the transmigration process, and therefore should be a non-contact or minimally-invasive measurement.

In order to address the question of whether tumor cells alter their mechanical properties during the

process of TEM, we apply two recently developed non-contact optical methods, Brillouin confocal microscopy (BCM) and confocal reflectance quantitative phase microscopy (QPM), to measure cell mechanical properties of the tumor cell and its nucleus in a 3D multi-cellular planar monolayer assay (Figure 1). BCM uses Brillouin light scattering to quantify intracellular longitudinal modulus without disturbing the cell (Nikolić and Scarcelli, 2019; Scarcelli et al., 2015) and recent work has shown this method can measure moduli of the nucleus inside cells with high spatial resolution (Wisniewski et al., 2020; Zhang et al., 2020). In contrast, confocal reflectance QPM, uses interferometry to measure the magnitude of thermal nuclear membrane fluctuations (Singh et al., 2019). While BCM and QPM measure different aspects of nuclear mechanics, their measurements provide new insight into the changes that occur in nuclear modulus during transendothelial migration.

2. Methods

2.1 Cell Culture

Human umbilical vein endothelial cells (Lonza) expressing mCherry LifeAct grew in culture in VascuLife basal media supplemented with VEGF LifeFactors (Lifeline) in 50µl/ml collagen I coated flasks. The metastatic tumor cells MDA-MB-231 (breast), A549 (lung), and A375 (melanoma, ATCC) grew in culture in DMEM supplemented with 10% FBS, 1% penicillin/streptomycin and 1% L-glutamate (Sigma). All cells were cultured in an incubator at 5% CO_2 at 37ºC.

2.2 Transendothelial Migration (TEM) Assay

After preparing a 2.5 mg/ml pH 7.4 rat-tail collagen I solution (Corning) on ice, we injected the gel into the 14mm diameter glass bottom well of a MatTek (P35G-0-14-C, MatTek) dish or on the

mirror glass bottom inside 9mm diameter silicone rings (666505, Grace BioLabs) for QPM measurements, generating a thin (~100 μm) layer. After the collagen polymerized at 37ºC in the incubator for 30 minutes, we seeded 100,000 HUVECs/ml onto the collagen gel surfaces. We provided the assays with fresh supplemented VascuLife medium after initial cell attachment and daily thereafter.

To begin a TEM experiment (Figure 1A), we harvested tumor cells, stained the nuclei with 1:2000 Hoechst (33342, ThermoFisher) in PBS and seeded onto the confluent HUVEC monolayer at a 3 x 10^5 cell/ml concentration. The time is noted as the initial time for the extravasation events. For Brillouin experiments, epifluorescence enabled identification of cell state (pre-extravasation, in-process, or extravasated) by morphological change previously confirmed with confocal fluorescence imaging (Figure 1B). Before extravasation, tumor cells appear as spheres on top of the endothelial cells. During TEM, the round cell body remains above the monolayer, while part of the cell spreads out below the endothelial cells (as in Figure S1). After TEM, tumor cells are entirely flattened (no more roundness) below the HUVEC monolayer.

To measure cell mechanical properties independently of the TEM process we seeded MDA-MB-231 cells inside (3D), and on top of the collagen matrix (2D) in absence of endothelial cells. In the 2D condition cells were seeded directly on top of a polymerized 2.5mg/ml collagen type I. In the 3D condition, cells were mixed with the ice-cold liquid collagen at 7.4 pH, and immediately placed in the incubator at 37ºC for 30 min to allow the collagen to polymerize. Cell experiments were then performed within 1.5 hours.

2.3 Brillouin confocal microscopy (BCM)

The Brillouin confocal microscope (Figure 1C) consists of a commercial inverted microscope (IX81, Olympus) and a two-stage VIPA (virtually imaged phased array) based Brillouin spectrometer, which has been reported before (Scarcelli et al., 2015; Zhang et al., 2020). Briefly, 10 mW power from a 660nm continuous-wave laser (Torus, Laser Quantum, Inc) was focused into the cell through an objective lens (40x/0.6 NA, LUCPLFLN40X , Olympus), which provides a lateral resolution of ~0.7μm and axial resolution of ~ 2.5μm. The backscattered Brillouin light was collected by the same objective lens and sent into the Brillouin spectrometer via a single mode optical fiber. An EMCCD camera (iXon 897, Andor) was used to record the Brillouin spectrum with a dwell time of 50ms, and the Brillouin shift was derived by fitting the spectrum with a Lorentzian function. Two-dimensional Brillouin image was acquired by scanning the cell with a motorized translational stage in horizontal and/or vertical planes. The step size was 0.5μm. The Brillouin microscope was also integrated with a brightfield and fluorescent imaging modality such that the Brillouin image can be co-registered with the brightfield and fluorescent images for the same cell (see Figure S1 for more clarification). This enabled confirmation of the tumor cell state (before, during, or after TEM) in the multicellular system.

To separate the Brillouin shift measurements of nucleus from the rest of the cell in cases where co-registration with fluorescence images is not available (e.g. in vertical plane images), we analyzed the distribution of shifts inside the cell. Typically, the distribution of Brillouin shifts inside a cell has two main components corresponding to nucleus and cytoplasm (Zhang et al., 2017). We identified these two components by fitting the histogram from the Brillouin shift data of the cell with a sum of two normal distribution functions and used the average of the higher distribution as

the indicator of the average nuclear modulus (Figure S2). We confirmed the accuracy of this method by cross validating it against the average of nuclear Brillouin shift in images that were co-registered with the nuclear fluorescence, showing the deviation between the fluorescence and histogram method is on the order of the instrumental precision of Brillouin shift in each pixel (8.4 MHz) (Figure S3).

The longitudinal modulus $\boldsymbol{M' = \Omega_B{}^2 \cdot \lambda^2 \cdot \rho / 4n^2}$, where $\boldsymbol{\Omega_B}$ is the measured Brillouin shift, λ is the wavelength of the laser, and $\boldsymbol{n}$ and $\boldsymbol{\rho}$ are the refractive index and mass density of the sample, respectively. While both the refractive index and the density may vary with conditions, their ratio $\boldsymbol{\rho / n^2}$ was found to be constant within cells (Kim and Guck, 2020). Therefore, we here use the Brillouin shift to interpret the relative modulus change of cells under transendothelial migration. The high-frequency (GHz) longitudinal modulus detected by Brillouin technique is different from the quasi-static Young's modulus measured by traditional methods, such as atomic force microscopy. However, strong correlation between two moduli has been observed in many biological samples, indicating both moduli change in the same direction in these physiological and pathologic processes (Scarcelli et al., 2015). Therefore, with prior calibration, Brillouin-derived modulus can be interpreted in terms of Young's modulus in some cases. For live cells, a log-log linear relationship between Brillouin-derived longitudinal modulus $\boldsymbol{M'}$ and Young's modulus $\boldsymbol{E'}$ measured by atomic force microscopy has been empirically determined as $\boldsymbol{log(M') = a\, log(E') + b}$. Thus, the relative change of the Young's modulus and the Brillouin shift are related by $\boldsymbol{\delta E'/E' = (2/a) \cdot \delta\Omega_B/\Omega_B}$, and the value of the coefficient $\boldsymbol{a}$ was previously calibrated as 0.0671 with NIH 3T3 cells. Here, we will also use this empirical relationship to estimate the relative change of Young's modulus based on measured Brillouin shifts.

2.4 Confocal reflectance quantitative phase microscopy (QPM)

Confocal reflectance QPM measures nanometer-scale thermally-driven nucleic and plasma membrane fluctuations with high sensitivity. Light from a 532nm laser light source (opus 532 from Laser Quantum) passes through a DMD (DLP discovery 4100 from Texas Instruments), creating a diffraction-limited size pinhole array and incident on the sample. The backscattered light from the sample passes back through the DMD, for confocal detection, followed by interferometric detection. In this multi-point scanning confocal reflectance interferometric microscope, foci size at the sample plane is 1.02 μm and system provides 1.5 μm axial resolution. The DMD scanning speed is 22 kHz, which provide the full field measurement speed at 14 ms.

The specular reflection from the mirror, located at an off-focal plane, underneath the sample, generates the highly phase-stabilized reference field. The common-path interferometry at the detection arm (shown in Figure 1D) provides the detection of optical phase information of the back scattered signal from nucleic membranes with height measurement accuracy better than 200 pm. For common path interferometer design, a transmission grating (with 80 line pairs per mm), placed at the image plane, diffracts the signal beam into 0 and +1 orders and generate the two copies of field incident on it. A DMD, located at the Fourier plane, allows the 0th order light to pass and create the object field. To generate the reference field, a COMB pattern spatial frequency filter (the Fourier transform of the pinhole array at the first image plane) is used for the +1 order, which provides the average phase of the object field. A CMOS sensor (Basler avA series) measures the interference pattern of the object and reference beams. A time series of wide-field

interferograms at the nuclear membrane was acquired and converted into height maps of temporal fluctuations.

The nuclear membrane regions of cells with sufficient signal-to-noise ratio were analyzed by employing the previously published fluctuations measurement algorithm (Singh et al., 2019). The number of cells measured was limited due to increased noise in the system from the endothelial cells fluctuations and 3D collagen matrix.

2.5 Statistical analysis

Data were analyzed using MATLAB (Mathworks) or R. All two-group comparisons were conducted with two-sample t-tests. Larger multi-group comparisons were achieved with one-way ANOVA tests followed by post-hoc Tukey's tests.

3. Results

3.1 Brillouin microscopy shows softening of tumor cells and their nuclei during and after TEM

We acquired 2D Brillouin images of tumor cells before, during, and after TEM. The three metastatic human tumor cell lines measured are derived from different kinds of cancer, all of which involve metastasis into the extracellular matrix from the blood stream. As A549 and A375 originated from the primary tumor site, the transendothelial migration observed in this work is the first extravasation event for these cells. The MDA-MB-231 tumor cell line differs in that it came from a secondary metastatic site in the lung and is mesenchymal. The A549 (lung) is the most invasive, followed by MDA-MB-231 (breast), and A375 (skin) (Vilalta et al., 2014; Xu et al., 2016).

These measurements exhibited a decrease in the Brillouin shift as TEM progressed, especially in the nuclear region. Figure 2A shows the colormaps of Brillouin frequency shift for MDA-MB-231 tumor cells before, during, and after TEM in the *z*-direction. As tumor cells crossed the endothelial monolayer, both the cells and most notably the nuclei softened. TEM typically occurred during a period of 2-8 hours. All three cell line types (A549, A375, MDA-MB-231) showed a significant difference in the Brillouin shift in the cell region between the before and after TEM populations (Figure 2B). We did not observe the alteration of the mechanical properties of the endothelial layer during TEM process (Figure S5). Based on the relationship between Young's modulus and the longitudinal modulus (Scarcelli et al., 2015), the Brillouin frequency shift changes (- 64 MHz, - 42 MHz, -41 MHz) correspond to a 30% (A549 nuclei), 20% (A375 nuclei), and 20% (MDA-MB-231 nuclei) reduction in Young's modulus from before to after TEM, respectively. Some of the cell softening occurred while the cell was in the process of crossing the endothelial monolayer. In-process A549 and A375 cells were significantly softer than cells before TEM (26 and 25 MHz Brillouin shift reduction correspond to approximately 12% reduction in Young's Modulus for each), suggesting tumor cells start softening during transendothelial migration. A549 and MDA-MB-231 in-process cells were also significantly stiffer than extravasated cells (40 MHz and 29 MHz Brillouin shift reduction, correspond to 18% and 14% reduction in Young's Modulus), respectively, supporting the claim that softening continued while tumor cells were crossing the endothelial monolayer.

Analysis of the nuclear regions of these tumor cells furthermore revealed significant softening of the nucleus during extravasation (Figure 2C). A549, A375, and MDA-MB-231 tumor cell nuclei after TEM presented significantly lower Brillouin shift. The Brillouin frequency shift changes -68

MHz (A549), -44 MHz (A375), and -53 MHz (MDA-MB-231) correspond to a 32% (A549 nuclei), 21% (A375 nuclei), and 25% (MDA-MB-231 nuclei) reduction in Young's modulus, respectively, from before to after TEM.

In summary, these Brillouin confocal microscopy experiments revealed that these three tumor cell lines (MDA-MB-231, A549, and A375) experienced a reduction in Brillouin shift in the cell, especially in the nucleus, during the process of transendothelial migration, indicating that tumor cells soften during the process of extravasation.

To investigate if the observed change in cell mechanics was due to the cell response to change in the external geometry experienced before and after TEM, we measured the Brillouin shift of MDA-MB-231 cells on top of a collagen surface (2D) and embedded inside a collagen gel (3D) (Figure 3A). We compared these 2D and 3D measurements with the prior experimental dataset of MDA-MB-231 cells before, during and after TEM (Figure 3B,C, and S4). The cells and nuclei before extravasation were notably softer than the 2D case. This may be due to differences in stiffness between the collagen substrate and the endothelial monolayer, which would influence the mechanical properties of the tumor cells, with cells on stiff substrates becoming less compliant (Wullkopf et al., 2018). By contrast, in another study (Abidine et al., 2018), it was found that tumor cells are stiffer on an endothelial cell monolayer than on an 8 kPa gel surface. There are several possible explanations for this discrepancy, however, including the lower stiffness of our collagen gel compared to the polyacrylamide gels used in the Abidine study, as well as the challenges associated with using AFM to measure cell and nuclear stiffness in a non-perturbative way.

While we had previously observed that Brillouin shift decreases as cells enter the 3D collagen gel during TEM, here we found that MDA-MB-231 cells seeded inside 3D collagen gel (without endothelial cells and the TEM process) have consistently higher Brillouin shifts than cells in 2D on top of the collagen surface (2D) (Figure 3). This finding aligns with previous studies of metastatic cancer cell mechanics in relation to 2D versus 3D collagen environment (Mak et al., 2014; Staunton et al., 2016). These results show that the MDA-MB-231 cell softening is a consequence of the mechanical and/or biochemical interaction with the endothelium during TEM, and not due to the 3D collagen gel environment.

3.2 QPM measurements show nuclear membranes soften after TEM

To further study whether tumor cells modulate their mechanical properties during TEM and if these changes persist, we used confocal reflectance quantitative phase microscopy (QPM). This complementary approach enabled quantification of the nuclear membrane fluctuations of tumor cells within the first hour of contact with the endothelial monolayer (pre-extravasation, Figure 4A, left) and tumor cells in the same sample 24 hours later after extravasation into the collagen gel (Figure 4A, right). The later time point ensured that all tumor cells measured not only had extravasated, but also were farther into the collagen away from the fluctuations of the endothelial cell membranes.

Figure 4B shows representative root mean square (rms) fluctuation maps of A549 tumor cells before and after extravasation. The A549 lung carcinoma cells 24 hours after extravasation showed dramatically higher nuclear fluctuations (approximately a 2.4-fold increase) than the same cells before extravasation. (Figure 4C). Hence, the membranes and/or the nuclear chromatin and cytoskeleton of tumor cells were more compliant after they extravasated into the collagen gel. For

A375 melanoma cells, however, the change in nuclear fluctuations between the pre-extravasation was not significant ($p = 0.053$).

4. Discussion

This study presents the first known experimental observations of a modulation in mechanical properties of tumor cells and their nuclei during transendothelial migration. We have observed this alteration to occur during transendothelial migration and to persist at least 24 hours. Two non-perturbative confocal methods, Brillouin confocal microscopy and confocal reflectance quantitative phase microscopy, enabled these intracellular measurements in a 3D TEM assay that maintained cell-cell and cell-collagen interactions. Although neither of these optical methods permits direct conversion to Young's modulus, they do non-invasively yield relative measurements of stiffness inside cells in 3D ECM-like microenvironments. BCM quantifies the Brillouin frequency shift, which is directly proportional to the longitudinal modulus and has been shown to correlate with Young's modulus for biological materials including cells (Scarcelli et al., 2011; Scarcelli et al., 2015). In the case of QPM, no model has been developed yet to directly link nuclear fluctuations to a modulus value. As a result, both BCM and QPM are best used for comparison of changes in mechanical properties rather than absolute values.

BCM and QPM are particularly complementary in noninvasively providing information about internal mechanical properties of cells during TEM and what parts may be contributing to the overall alteration in stiffness. The results show that the Brillouin shift of A549, A375 and MDA-MB-231 tumor cells and their nuclei decrease as they migrate across the endothelial monolayer. This observed modulation of stiffness of MDA-MB-231 cells is not due to the transition from a

suspended state to a state embedded in 3D collagen (Figure 3), but rather due to the process of TEM, which incorporates tumor cell – endothelial cell interactions. Changes in the chromatin structure rather than changes in the nuclear membrane properties are mostly likely to contribute to this alteration in stiffness inside the tumor cell nuclei, since the changes appear throughout the nuclear volume. Chromatin decompaction is known to soften cells (Stephens et al., 2017; Stephens et al., 2018) and likely drives our observed modulation in Brillouin shift in the nuclear region as demonstrated by Zhang (Zhang et al., 2020).

Measurements of nuclear membrane fluctuations from QPM show a marked increase in A549 tumor cells, demonstrating either a reduction in modulus of the external cytoskeleton, internal chromatin or the nuclear membrane or a combination. In addition, they show that the changes in A549 tumor cells persist even 24 hours after endothelial contact. This further supports the Brillouin data that shows a softening of the extravasated A549 nuclei and suggests that the softening effect is longer term. While nuclear rupture could explain an increase in nuclear membrane fluctuations, this event is rare and would likely cause a more significant effect than observed here. This measurement is not only dependent on the inherent stiffness of the membrane, but also the modulus on either side of the nuclear membrane. As BCM reveals the intranuclear softening, we hypothesize that the nuclear membrane fluctuations are increasing due to softening inside the nucleus and result from changes in chromatin structure during TEM. Our findings align with recent AFM work showing that tumor cells soften when migrating into confined spaces (Rianna et al., 2020). Observations from that study also suggest that nuclear exclusion of YAP may contribute to nuclear softening. Additionally, cell cycle phase may play a role in the observed softening. During the S/G2 cell cycle phase, chromatin decondense and tumor cell nuclei soften (Krause et al., 2019). During and/or after

transendothelial migration, tumor cells may be softening due to transition into the S/G2 phase.

Future work will be required to understand the mechanisms by which tumor cells soften during TEM. Partial wave spectroscopy may be a valuable tool in assessing chromatin condensation for this application, although the method is currently best applied to samples in 2D on glass (Stephens et al., 2018). While, the implications of changes in the chromatin structure may be vast, more work is required to prove that chromatin alterations cause the change in stiffness we observe during TEM.

While many models of extravasation exist, none account for a change in nuclear stiffness during this event. New models incorporating this finding may present new understanding in how tumor cells metastasize. The softening of tumor cell nuclei may enable the process of TEM, as well as affect processes in later steps of metastasis. As softer tumor cells are known to be more metastatic (Guck et al., 2005), the lasting softening effect observed in A549 lung carcinoma cells may enable further migration into the extracellular matrix and suggest a continued proliferative phenotype. Furthermore, a recent study showed that softer melanoma cells metastasized to the lungs and formed significantly more tumors *in vivo* than stiffer cells (Lv et al., 2021). Also, potential increase in euchromatin likely correlate with further transcriptional alterations (Rochman et al., 2009), which may promote metastasis or influence the subsequent fate of a tumor cell at the metastatic site. The softening of the nucleus likely plays an important role in facilitating the metastasis of tumor cells, but more experimental and theoretical work will be needed to shed light on the underlying mechanisms.

Conflict of interest

RK is Co-founder of AIM Biotech with significant financial interests and has research agreements with Biogen, Amgen and Gore. GS has intellectual property related to Brillouin microscopy and has equity in Intelon Optics.

Acknowledgements

This research was supported by the National Cancer Institute (U01 CA202177, R33CA204582) and the National Science Foundation (CMMI 1929412).

References

Abidine, Y., Constantinescu, A., Laurent, V.M., Rajan, V.S., Michel, R., Laplaud, V., Duperray, A., Verdier, C., 2018. Mechanosensitivity of cancer cells in contact with soft substrates using AFM. Biophysical Journal 114(5), pp. 1165-1175.

Caille, N., Thoumine, O., Tardy, Y., Meister, J.-J., 2002. Contribution of the nucleus to the mechanical properties of endothelial cells. Journal of Biomechanics 35(2), pp. 177-187.

Cao, X., Moeendarbary, E., Isermann, P., Davidson, P.M., Wang, X., Chen, M.B., Burkart, A.K., Lammerding, J., Kamm, R.D., Shenoy, V.B., 2016. A chemomechanical model for nuclear morphology and stresses during cell transendothelial migration. Biophysical Journal 111(7), pp. 1541-1552.

Chen, M.B., Lamar, J.M., Li, R., Hynes, R.O., Kamm, R.D., 2016. Elucidation of the roles of tumor integrin β1 in the extravasation stage of the metastasis cascade. Cancer Research 76(9), pp. 2513-2524.

Chen, M.B., Whisler, J.A., Fröse, J., Yu, C., Shin, Y., Kamm, R.D., 2017. On-chip human microvasculature assay for visualization and quantification of tumor cell extravasation dynamics. Nature Protocols 12(5), pp. 865-880.

Cross, S.E., Jin, Y.-S., Rao, J., Gimzewski, J.K., 2007. Nanomechanical analysis of cells from cancer patients. Nature nanotechnology 2(12), pp. 780-783.

Dahl, K.N., Engler, A.J., Pajerowski, J.D., Discher, D.E., 2005. Power-law rheology of isolated nuclei with deformation mapping of nuclear substructures. Biophysical Journal 89(4), pp. 2855-2864.

Davidson, P.M., Denais, C., Bakshi, M.C., Lammerding, J., 2014. Nuclear deformability constitutes

a rate-limiting step during cell migration in 3-D environments. Cellular and Molecular Bioengineering 7(3), pp. 293-306.

Davidson, P.M., Sliz, J., Isermann, P., Denais, C., Lammerding, J., 2015. Design of a microfluidic device to quantify dynamic intra-nuclear deformation during cell migration through confining environments. Integrative Biology 7(12), pp. 1534-1546.

Deguchi, S., Maeda, K., Ohashi, T., Sato, M., 2005. Flow-induced hardening of endothelial nucleus as an intracellular stress-bearing organelle. Journal of Biomechanics 38(9), pp. 1751-1759.

Deguchi, S., Yano, M., Hashimoto, K., Fukamachi, H., Washio, S., Tsujioka, K., 2007. Assessment of the mechanical properties of the nucleus inside a spherical endothelial cell based on microtensile testing. Journal of Mechanics of Materials and Structures 2(6), pp. 1087-1102.

Denais, C., Lammerding, J., 2014. Nuclear mechanics in cancer, in: Eric C. Schirmer, J.I.d.l.H. (Ed.), Cancer Biology and the Nuclear Envelope. Springer, New York, NY, pp. 435-470.

Denais, C.M., Gilbert, R.M., Isermann, P., McGregor, A.L., Te Lindert, M., Weigelin, B., Davidson, P.M., Friedl, P., Wolf, K., Lammerding, J., 2016. Nuclear envelope rupture and repair during cancer cell migration. Science 352(6283), pp. 353-358.

Escribano, J., Chen, M.B., Moeendarbary, E., Cao, X., Shenoy, V., Garcia-Aznar, J.M., Kamm, R.D., Spill, F., 2019. Balance of mechanical forces drives endothelial gap formation and may facilitate cancer and immune-cell extravasation. PLoS Computational Biology 15(5), p. e1006395.

Friedl, P., Wolf, K., Lammerding, J., 2011. Nuclear mechanics during cell migration. Current Opinion in Cell Biology 23(1), pp. 55-64.

Guck, J., Schinkinger, S., Lincoln, B., Wottawah, F., Ebert, S., Romeyke, M., Lenz, D., Erickson, H.M., Ananthakrishnan, R., Mitchell, D., 2005. Optical deformability as an inherent cell marker for testing malignant transformation and metastatic competence. Biophysical Journal 88(5), pp. 3689-3698.

Guilak, F., Tedrow, J.R., Burgkart, R., 2000. Viscoelastic properties of the cell nucleus. Biochemical and Biophysical Research Communications 269(3), pp. 781-786.

Han, Y.L., Pegoraro, A.F., Li, H., Li, K., Yuan, Y., Xu, G., Gu, Z., Sun, J., Hao, Y., Gupta, S.K., 2020. Cell swelling, softening and invasion in a three-dimensional breast cancer model. Nature physics 16(1), pp. 101-108.

Harada, T., Swift, J., Irianto, J., Shin, J.-W., Spinler, K.R., Athirasala, A., Diegmiller, R., Dingal, P.D.P., Ivanovska, I.L., Discher, D.E., 2014. Nuclear lamin stiffness is a barrier to 3D migration, but softness can limit survival. Journal of Cell Biology 204(5), pp. 669-682.

Herráez-Aguilar, D., Madrazo, E., López-Menéndez, H., Ramírez, M., Monroy, F., Redondo-Muñoz, J., 2020. Multiple particle tracking analysis in isolated nuclei reveals the mechanical phenotype of leukemia cells. Scientific Reports 10(1), pp. 1-12.

Kale, V.P., Hengst, J.A., Desai, D.H., Amin, S.G., Yun, J.K., 2015. The regulatory roles of ROCK and MRCK kinases in the plasticity of cancer cell migration. Cancer Letters 361(2), pp. 185-196.

Kim, K., Guck, J., 2020. The relative densities of cytoplasm and nuclear compartments are robust against strong perturbation. Biophysical Journal 119(10), pp. 1946-1957.

Krause, M., Yang, F.W., Te Lindert, M., Isermann, P., Schepens, J., Maas, R.J., Venkataraman, C., Lammerding, J., Madzvamuse, A., Hendriks, W., 2019. Cell migration through three-dimensional confining pores: speed accelerations by deformation and recoil of the nucleus. Philosophical Transactions of the Royal Society B 374(1779), p. 20180225.

Liu, H., Wen, J., Xiao, Y., Liu, J., Hopyan, S., Radisic, M., Simmons, C.A., Sun, Y., 2014. In situ mechanical characterization of the cell nucleus by atomic force microscopy. ACS nano 8(4), pp. 3821-3828.

Lombardi, M.L., Jaalouk, D.E., Shanahan, C.M., Burke, B., Roux, K.J., Lammerding, J., 2011. The interaction between nesprins and sun proteins at the nuclear envelope is critical for force transmission between the nucleus and cytoskeleton. Journal of Biological Chemistry 286(30), pp. 26743-26753.

Lv, J., Liu, Y., Cheng, F., Li, J., Zhou, Y., Zhang, T., Zhou, N., Li, C., Wang, Z., Ma, L., 2021. Cell softness regulates tumorigenicity and stemness of cancer cells. The EMBO journal 40(2), p. e106123.

Mak, M., Kamm, R.D., Zaman, M.H., 2014. Impact of dimensionality and network disruption on microrheology of cancer cells in 3D environments. PLoS Computational Biology 10(11), p. e1003959.

Nikolić, M., Scarcelli, G., 2019. Long-term Brillouin imaging of live cells with reduced absorption-mediated damage at 660nm wavelength. Biomedical optics express 10(4), pp. 1567-1580.

Reymond, N., Im, J.H., Garg, R., Cox, S., Soyer, M., Riou, P., Colomba, A., Muschel, R.J., Ridley, A.J., 2015. RhoC and ROCKs regulate cancer cell interactions with endothelial cells. Molecular Oncology 9(6), pp. 1043-1055.

Rianna, C., Radmacher, M., Kumar, S., 2020. Direct evidence that tumor cells soften when navigating confined spaces. Molecular Biology of the Cell 31(16), pp. 1726-1734.

Ribeiro, A.J., Khanna, P., Sukumar, A., Dong, C., Dahl, K.N., 2014. Nuclear stiffening inhibits migration of invasive melanoma cells. Cellular and Molecular Bioengineering 7(4), pp. 544-551.

Rochman, M., Postnikov, Y., Correll, S., Malicet, C., Wincovitch, S., Karpova, T.S., McNally, J.G., Wu, X., Bubunenko, N.A., Grigoryev, S., 2009. The interaction of NSBP1/HMGN5 with nucleosomes in euchromatin counteracts linker histone-mediated chromatin compaction and modulates transcription. Molecular Cell 35(5), pp. 642-656.

Rowat, A.C., Jaalouk, D.E., Zwerger, M., Ung, W.L., Eydelnant, I.A., Olins, D.E., Olins, A.L.,

Herrmann, H., Weitz, D.A., Lammerding, J., 2013. Nuclear envelope composition determines the ability of neutrophil-type cells to passage through micron-scale constrictions. Journal of Biological Chemistry 288(12), pp. 8610-8618.

Scarcelli, G., Kim, P., Yun, S.H., 2011. In vivo measurement of age-related stiffening in the crystalline lens by Brillouin optical microscopy. Biophysical Journal 101(6), pp. 1539-1545.

Scarcelli, G., Polacheck, W.J., Nia, H.T., Patel, K., Grodzinsky, A.J., Kamm, R.D., Yun, S.H., 2015. Noncontact three-dimensional mapping of intracellular hydromechanical properties by Brillouin microscopy. Nature methods 12(12), pp. 1132-1134.

Singh, V.R., Yang, Y.A., Yu, H., Kamm, R.D., Yaqoob, Z., So, P.T., 2019. Studying nucleic envelope and plasma membrane mechanics of eukaryotic cells using confocal reflectance interferometric microscopy. Nature communications 10(1), pp. 1-8.

Staunton, J.R., Doss, B.L., Lindsay, S., Ros, R., 2016. Correlating confocal microscopy and atomic force indentation reveals metastatic cancer cells stiffen during invasion into collagen I matrices. Scientific Reports 6(1), pp. 1-15.

Stephens, A.D., Banigan, E.J., Adam, S.A., Goldman, R.D., Marko, J.F., 2017. Chromatin and lamin A determine two different mechanical response regimes of the cell nucleus. Molecular Biology of the Cell 28(14), pp. 1984-1996.

Stephens, A.D., Liu, P.Z., Banigan, E.J., Almassalha, L.M., Backman, V., Adam, S.A., Goldman, R.D., Marko, J.F., 2018. Chromatin histone modifications and rigidity affect nuclear morphology independent of lamins. Molecular Biology of the Cell 29(2), pp. 220-233.

Swaminathan, V., Mythreye, K., O'Brien, E.T., Berchuck, A., Blobe, G.C., Superfine, R., 2011. Mechanical stiffness grades metastatic potential in patient tumor cells and in cancer cell lines. Cancer Research 71(15), pp. 5075-5080.

Tseng, Y., Lee, J.S., Kole, T.P., Jiang, I., Wirtz, D., 2004. Micro-organization and visco-elasticity of the interphase nucleus revealed by particle nanotracking. Journal of Cell Science 117(10), pp. 2159-2167.

Vilalta, M., Rafat, M., Giaccia, A.J., Graves, E.E., 2014. Recruitment of circulating breast cancer cells is stimulated by radiotherapy. Cell Reports 8(2), pp. 402-409.

Wirtz, D., 2009. Particle-tracking microrheology of living cells: principles and applications. Annual review of biophysics 38), pp. 301-326.

Wisniewski, E.O., Mistriotis, P., Bera, K., Law, R.A., Zhang, J., Nikolic, M., Weiger, M., Parlani, M., Tuntithavornwat, S., Afthinos, A., 2020. Dorsoventral polarity directs cell responses to migration track geometries. Science advances 6(31), p. eaba6505.

Wolf, K., Te Lindert, M., Krause, M., Alexander, S., Te Riet, J., Willis, A.L., Hoffman, R.M., Figdor, C.G., Weiss, S.J., Friedl, P., 2013. Physical limits of cell migration: control by ECM space

and nuclear deformation and tuning by proteolysis and traction force. Journal of Cell Biology 201(7), pp. 1069-1084.

Wullkopf, L., West, A.-K.V., Leijnse, N., Cox, T.R., Madsen, C.D., Oddershede, L.B., Erler, J.T., 2018. Cancer cells' ability to mechanically adjust to extracellular matrix stiffness correlates with their invasive potential. Molecular Biology of the Cell 29(20), pp. 2378-2385.

Xu, H., Li, Z., Yu, Y., Sizdahkhani, S., Ho, W.S., Yin, F., Wang, L., Zhu, G., Zhang, M., Jiang, L., 2016. A dynamic in vivo-like organotypic blood-brain barrier model to probe metastatic brain tumors. Scientific Reports 6(1), pp. 1-12.

Yamada, S., Wirtz, D., Kuo, S.C., 2000. Mechanics of living cells measured by laser tracking microrheology. Biophysical Journal 78(4), pp. 1736-1747.

Zhang, J., Alisafaei, F., Nikolić, M., Nou, X.A., Kim, H., Shenoy, V.B., Scarcelli, G., 2020. Nuclear mechanics within intact cells is regulated by cytoskeletal network and internal nanostructures. Small 16(18), p. 1907688.

Zhang, J., Nou, X.A., Kim, H., Scarcelli, G., 2017. Brillouin flow cytometry for label-free mechanical phenotyping of the nucleus. Lab on a Chip 17(4), pp. 663-670.

Figure 1: Methods to study stiffness during transendothelial migration. **A**. In the assay, an endothelial monolayer (red) grows on top of a 2.5µg/ml collagen I matrix over 100µm in height. Tumor cells (green) are seeding into the media, attach to the endothelial cells, and transmigrate into the collagen matrix. **B**. Time-lapse confocal slices showing the tumor cell (A549-GFP, green) before extravasation, in process, and after transmigration across the endothelial monolayer (HUVEC-RFP, red). Nuclei (blue) are Hoechst-stained. **C**. The Brillouin Confocal Microscopy (BCM) measures brillouin shift via raster scan throughout the cell in 3D. MO is the mirror and objective. **D**. Quantitative Phase Microscopy (QPM) measures the fluctuations of the nuclear membrane. In the backscattering detection arm, a common-path interferometer, comprised of the grating, DMD-2 and spatial frequency filter, enables depth-resolved optical phase measurements of the nuclear membrane fluctuations. The camera collects the interferogram of the reference and object beams.

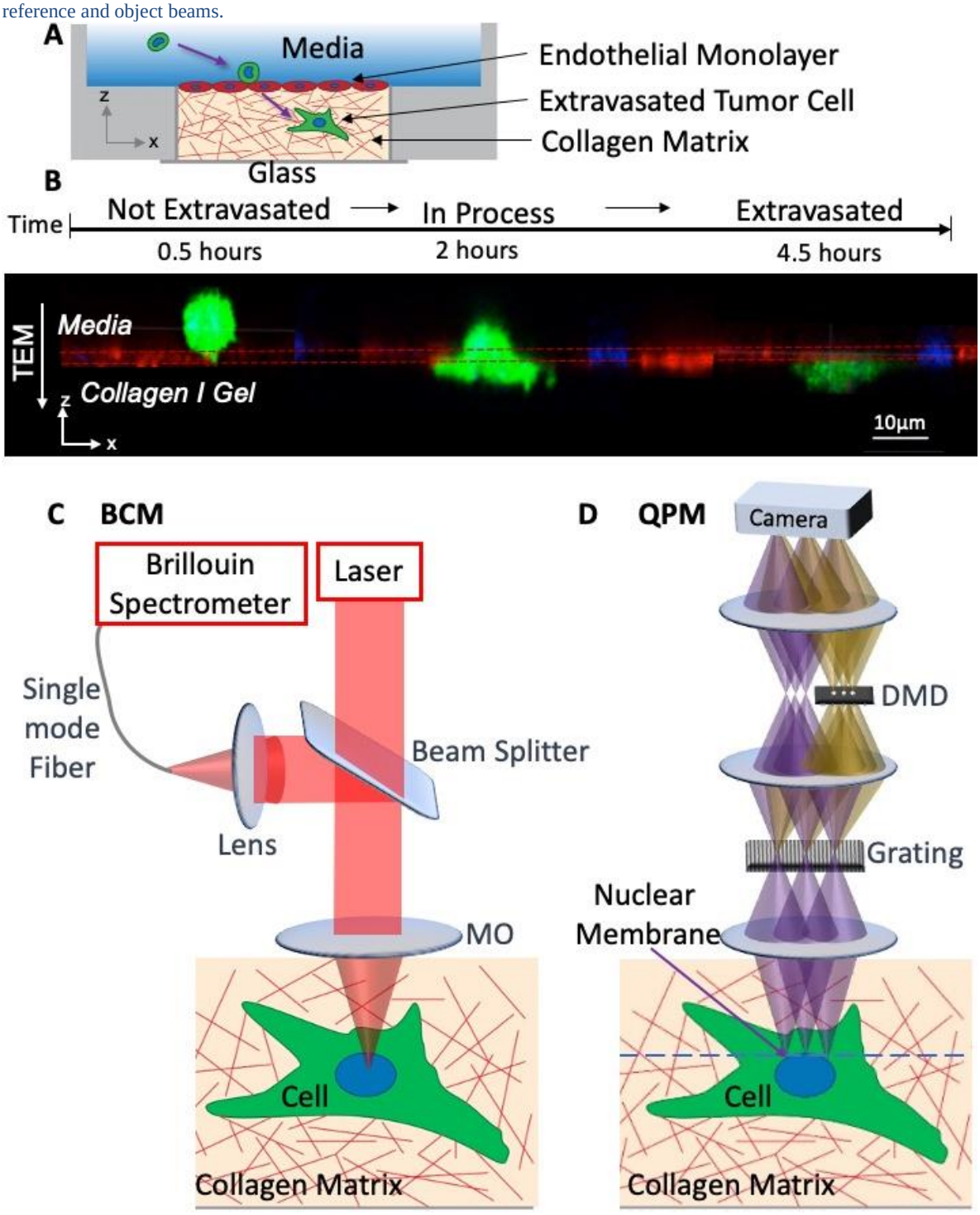

Figure 2: Tumor cells soften after transendothelial migration (TEM) according to Brillouin confocal microscopy. **A.** Brillouin shift image of an MDA-MB-231 tumor cell on top of the endothelial cell monolayer before TEM, between endothelial cells during TEM, and after TEM under the monolayer. Higher GHz shift (red) corresponds to stiffer material. Scale bars are 20µm long. **B.** Whole cell Brillouin shift (GHz) of A549, A375, and MDA-MB-231 cells before TEM (red), in-process of transendothelial migration (green), and after TEM (blue). Average Brillouin shifts for tumor cells before, during, and after TEM are: 6.34, 6.31, and 6.27 GHz (A549), 6.31, 6.28, and 6.27 GHz (A375), and 6.22, 6.21, and 6.18 GHz (MDA-MB-231). **C**. Brillouin Shift in the nuclear region of A549, A375, and MDA-MB-231 cells before TEM (red), in-process of transendothelial migration (green), and after TEM (blue). Average nuclear Brillouin shifts for tumor cells before, during, and after TEM are: 6.34, 6.31, and 6.27 GHz (A549), 6.31, 6.28, and 6.26 GHz (A375), and 6.27, 6.26, and 6.22 GHz (MDA-MB-231). Higher GHz shift corresponds to stiffer material. Post-hoc Tukey's test p-values of ≤0.01 and ≤ 0.001 are signified by ** and ***, respectively.

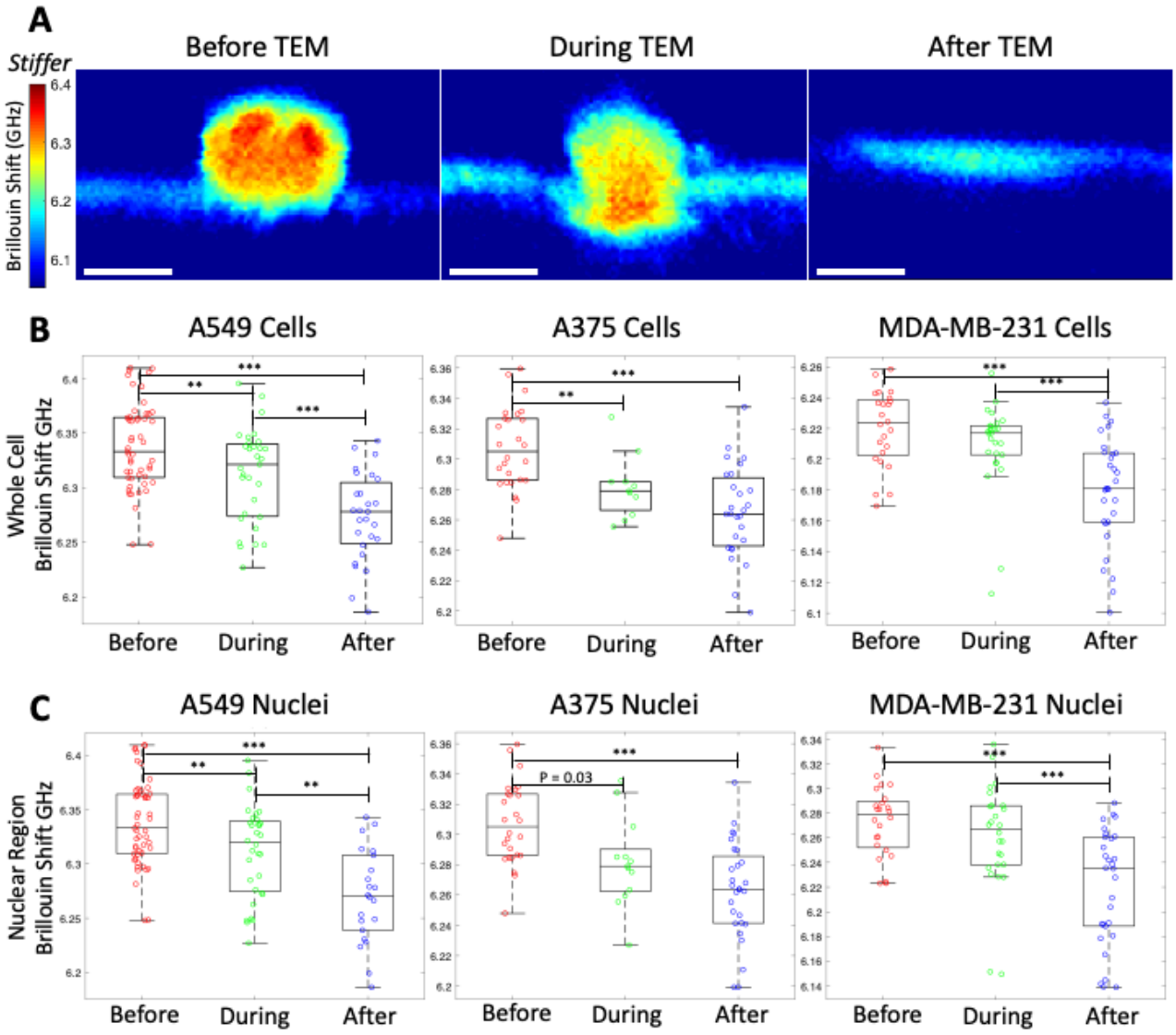

Figure 3: Tumor cells in 3D collagen I have higher Brillouin shift than in 2D on collagen. **A**. In the 2D case, MDA-MB-231 tumor cells were place in media on top of a collagen matrix. For 3D measurements, tumor cells were embedded in 2.5mg/ml rat tail collagen I. Brightfield images of 2D (left) and 3D (right) cells. Error bar is 10μm long. **B** and **C** Whole cell and nuclear (respectively) Brillouin shift measurements of MDA-MB-231 cells in 3D.(magenta), in 2D (cyan), and before (red), during (green), and after (blue) transendothelial migration. All data are normalized for comparison by subtracting the mean of the 2D measurements. Each circle represents a different cell. All post-hoc Tukey's tests were significant at $p < 0.001$, except as indicated. "ns" is not significant.

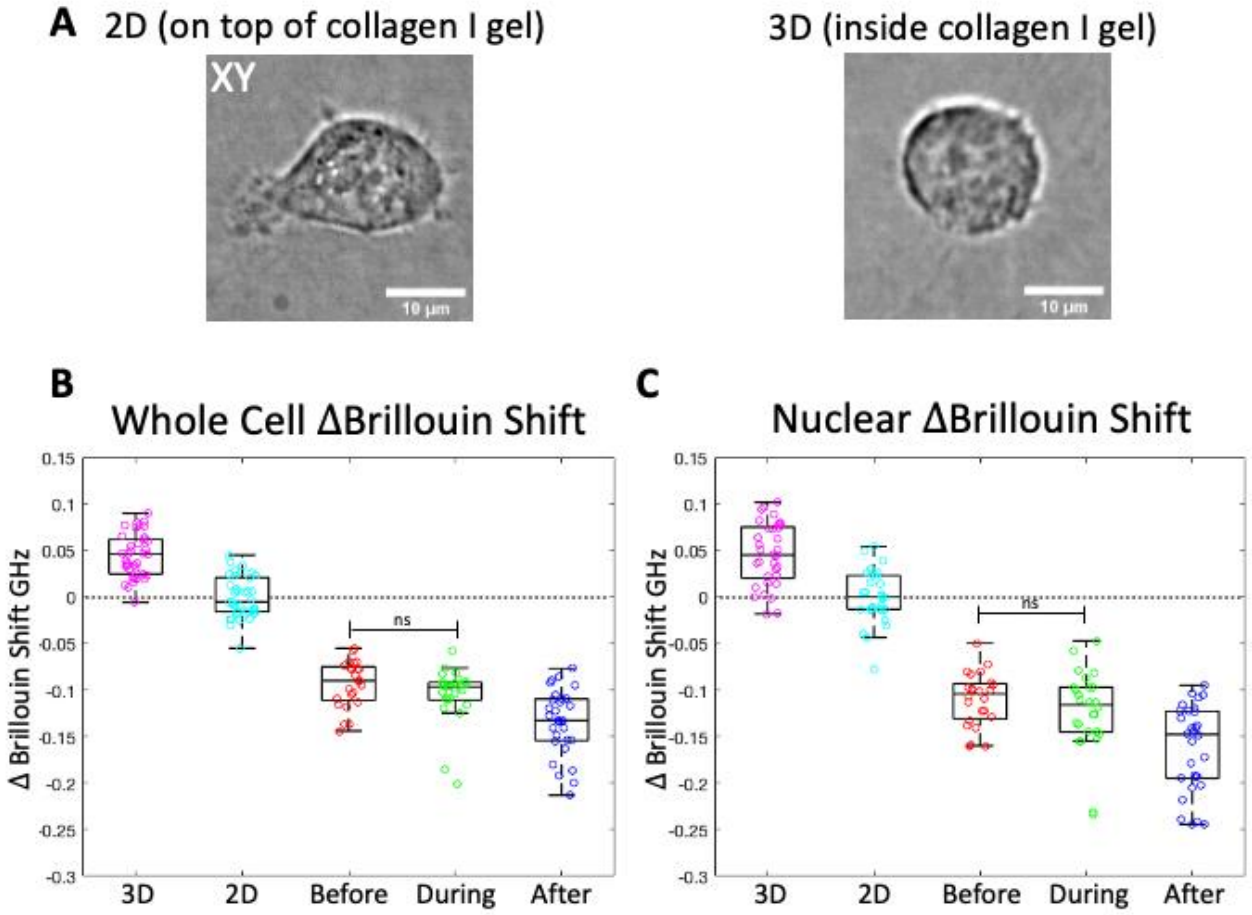

Figure 4: The nuclear membranes of tumor cells soften after transendothelial migration A. Nuclear fluctuations were measured at the tumor cell nuclear membrane interface (yellow dotted line) before transendothelial migration (TEM), right after the tumor cells attach to the endothelial wall (left), and 24 hours later after the TEM event has occurred (right). **B**. QPM maps of root mean square fluctuation heights (nm) of A549 cells before and after TEM. These fluctuations are recorded in the plane of the nuclear membrane. **C.** QPM nuclear fluctuations (nm) of A375 cells before extravasation and after extravasation (24 hours post endothelial contact). *** signifies $p \leq 0.001$ (2-sample t-test). **D**. QPM nuclear fluctuations (nm) of A375 cells before extravasation and after extravasation (24 hours post endothelial contact). P = 0.053 (2-sample t-test).

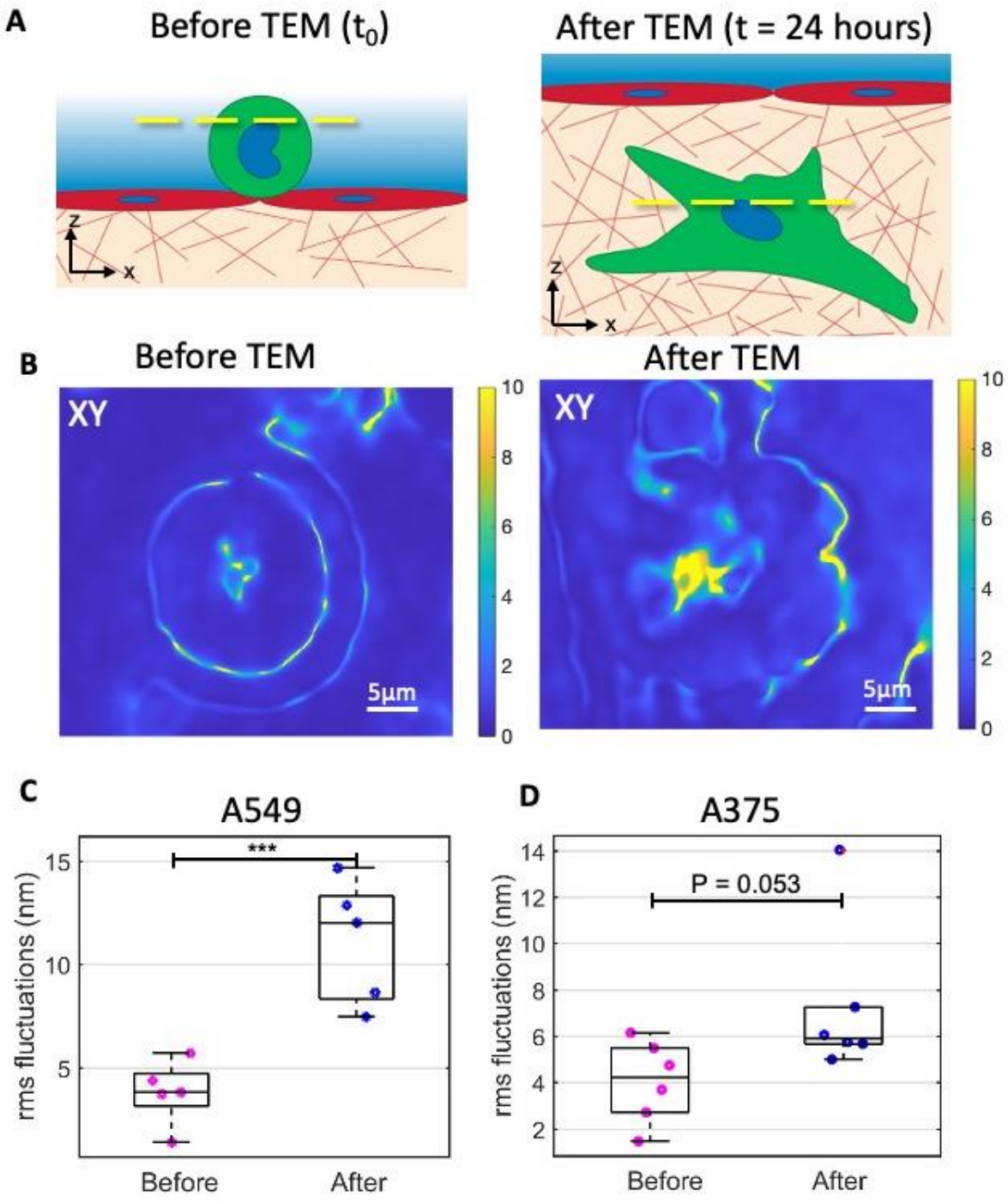

Tumor cell nuclei soften during transendothelial migration

Anya B. Roberts[1], Jitao Zhang[2], Vijay Raj Singh[3,4], Miloš Nikolić[5], Roger D. Kamm[†,1,3], Peter T. C. So[‡,1,3,4], Giuliano Scarcelli[*2,5]

[1]*Department of Biological Engineering, Massachusetts Institute of Technology, Cambridge, 02139, MA*
[2]*Fischell Department of Bioengineering, University of Maryland, College Park, 20742, MD*
[3]*Department of Mechanical Engineering, Massachusetts Institute of Technology, Cambridge, 02139, MA*
[4]*Laser Biomedical Research Center, Massachusetts Institute of Technology, Cambridge, 02139, MA*
[5]*Maryland Biophysics Program, University of Maryland, College Park, MD 20742, USA.*
[†]*rdkamm@mit.edu,* [‡]*ptso@mit.edu,*[*] *sarc@umd.edu*

Supplementary Figures:

Figure S1: Brillouin confocal microscopy images of a A549 tumor cell during TEM.

Figure S2: Histogram Analysis for A375 cells before, during and after TEM.

Figure S3: Validation of Histogram Analysis using Fluorescence Image Registration

Figure S4: MDA-MB-231 cells on 2D collagen I gel and embedded in 3D collagen I gel

Figure S1: Brillouin confocal microscopy images of a A549 tumor cell during TEM. A) An A549 lung carcinoma cell in the planar monolayer assay is in process of transendothelial migration in the - z-direction. The three xy epifluorescence images of the ROI show the nuclei (Hoechst, blue), the A549 (GFP, green), and the HUVEC monolayer below (LifeAct, red). The bar is 30µm long and the white circles indicate the immediate region of the cell of interest. In the inset image of the endothelial monolayer, a gap much smaller than 10µm. The tumor cell is in process of migration through this constriction, with part of the cell above and part below the endothelium. **B**) Epifluorescence images of the nuclei (left) and tumor cell (right) just before the BCM measurements shown in D). The horizontal red line shows the x-axis line along which BCM measurements were recorded (in the z above and below this plane). **C**) Epifluorescence images of the nuclei (left) and tumor cell (right) just before the BCM measurements shown in E). The red box encloses the xy region of the BCM measurements. Bars are 30µm long. **D**) Spatial Brillouin shift plot of the xz slice (marked in red in B) of the tumor cells in process of migrating through the endothelium (towards the collagen in the - z-direction). Redder regions indicate regions of higher stiffness (GHz Brillouin shift). The white dotted line marks the top of the endothelial monolayer. **E**) Spatial Brillouin shift plot of the same cell in the xy axes (region noted in red in C). Redder regions indicate regions of higher stiffness (GHz Brillouin shift). This image is 30µm x 30µm.

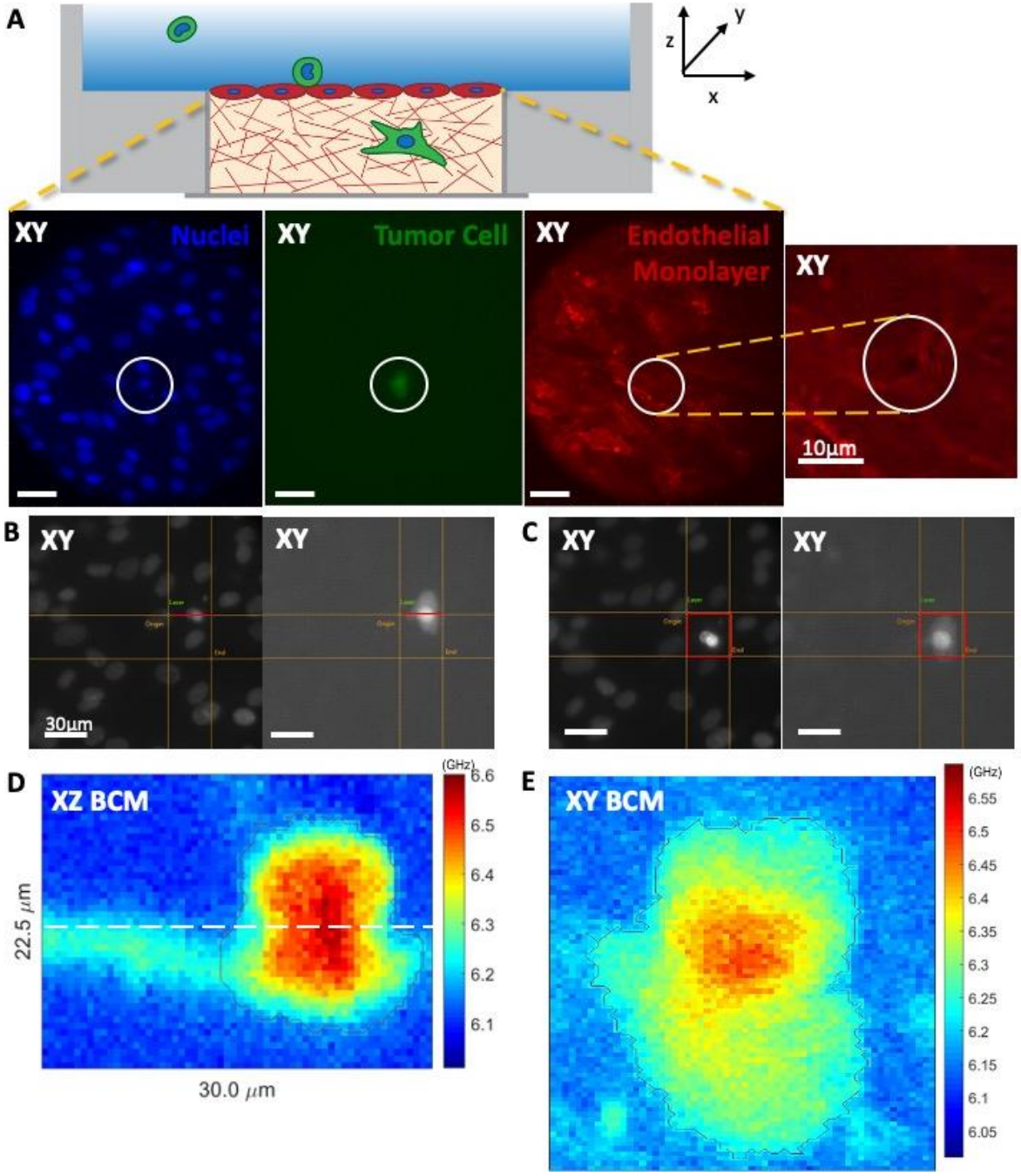

Figure S2: Histogram Analysis for A375 cells before, during and after TEM. The Brillouin image and histogram data for A375 cells before TEM (**A**), during TEM (**B**), and after TEM (**C**). Each Brillouin shift point in the histogram is a measured point from the encircled red cell region in the Brillouin image. The inner black region in the Brillouin images are the threshold for the nuclear region of that cell. The green dotted curve represents the signature of the cytoplasm and the blue dotted curve represents the signature of the nucleus. Scale bars are 10μm.

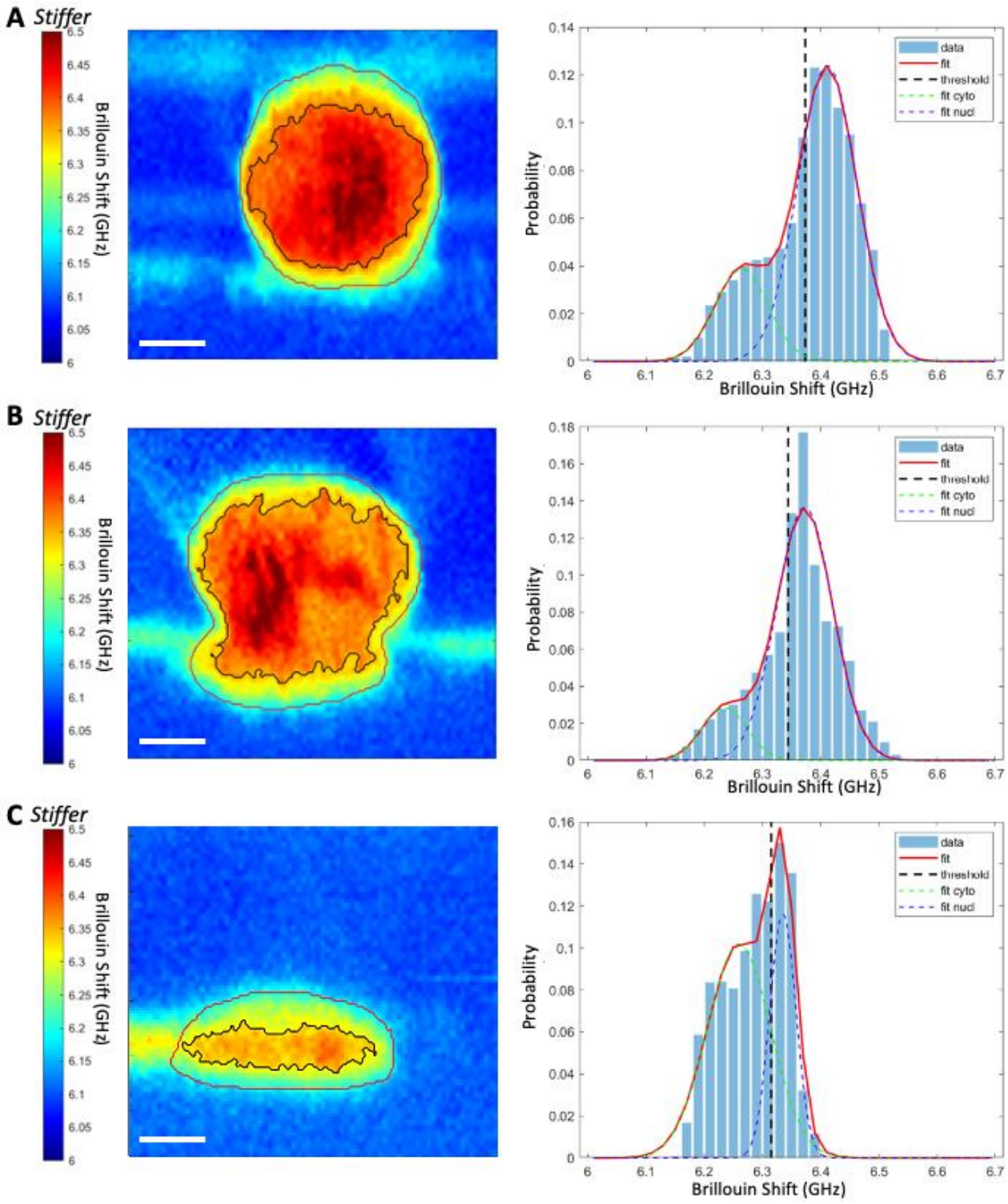

Figure S3: Validation of Histogram Analysis using Fluorescence Image Registration. (**A**) Bimodal (normal) distribution fit of the Brillouin shifts inside the cell. Black dashed line is a weighted average of the centers of the two normal distributions. (**B**) Widefield fluorescence image of a cell. The nucleus is blue and the whole cell tracker is green. Dashed lines indicate the boundaries of the nucleus (blue dashed line) and of the cell (green dashed line). (**C**) Co-registered Brillouin shift map with cell and nucleus boundaries determined as the contour at Brillouin shift that corresponds to the weighted average of the two centers of fitted normal distributions. (A). Black line represents the approximate threshold of the Brillouin shift map that separates the nucleus and cytoplasm. **(D)** Co-registered Brillouin shift map overlayed with nuclear fluorescence (blue). Green intensity represents the probability the pixel comes from the low-shift component (cytoplasm), and red intensity represents the probability the pixel comes from the high-shift component (nucleus). **(E)** Comparison of the distribution of nuclear shifts estimated from the bimodal fitting and true distribution of nuclear shifts (from fluorescence co-localization). **(F)** Plot of the nuclear shift estimated through two methods. Error bars are 0.008 GHz which a typical instrumental precision of Brillouin spectrometer. Black line is identity line. Scale bars are 10 μm.

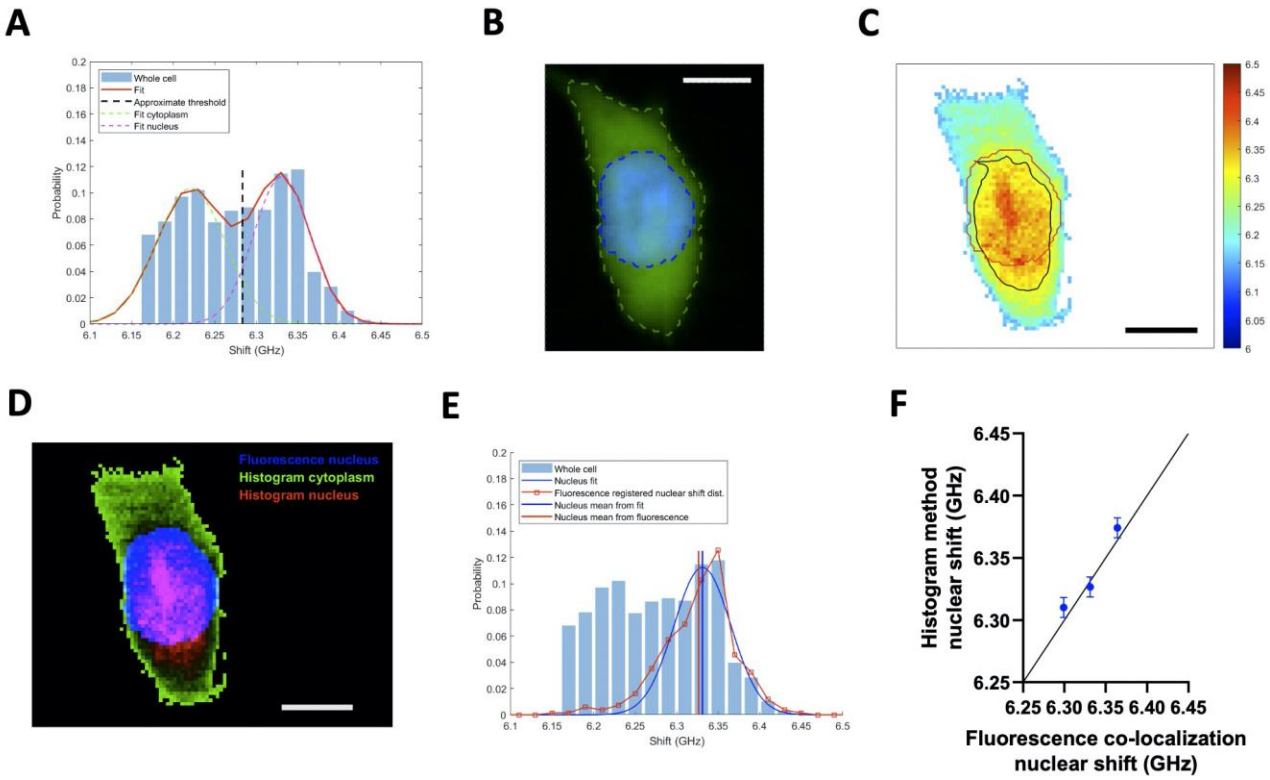

Figure S4: MDA-MB-231 cells on 2D collagen I gel and embedded in 3D collagen I gel. A. Left: whole cell BCM data for three experimental replicates of 2D (cyan) and 3D samples (magenta). Right: nuclear region BCM data for three experimental replicates of 2D and 3D samples. *** represents a p-value of < 0.001 (2-sample t-test). B. Whole cell BCM data for 3D (blue) and 2D (red) samples measured 0.5-1 hours after seeding and the same samples 24 hours later showed no significant difference in Brillouin shift over time (2 sample t-test).

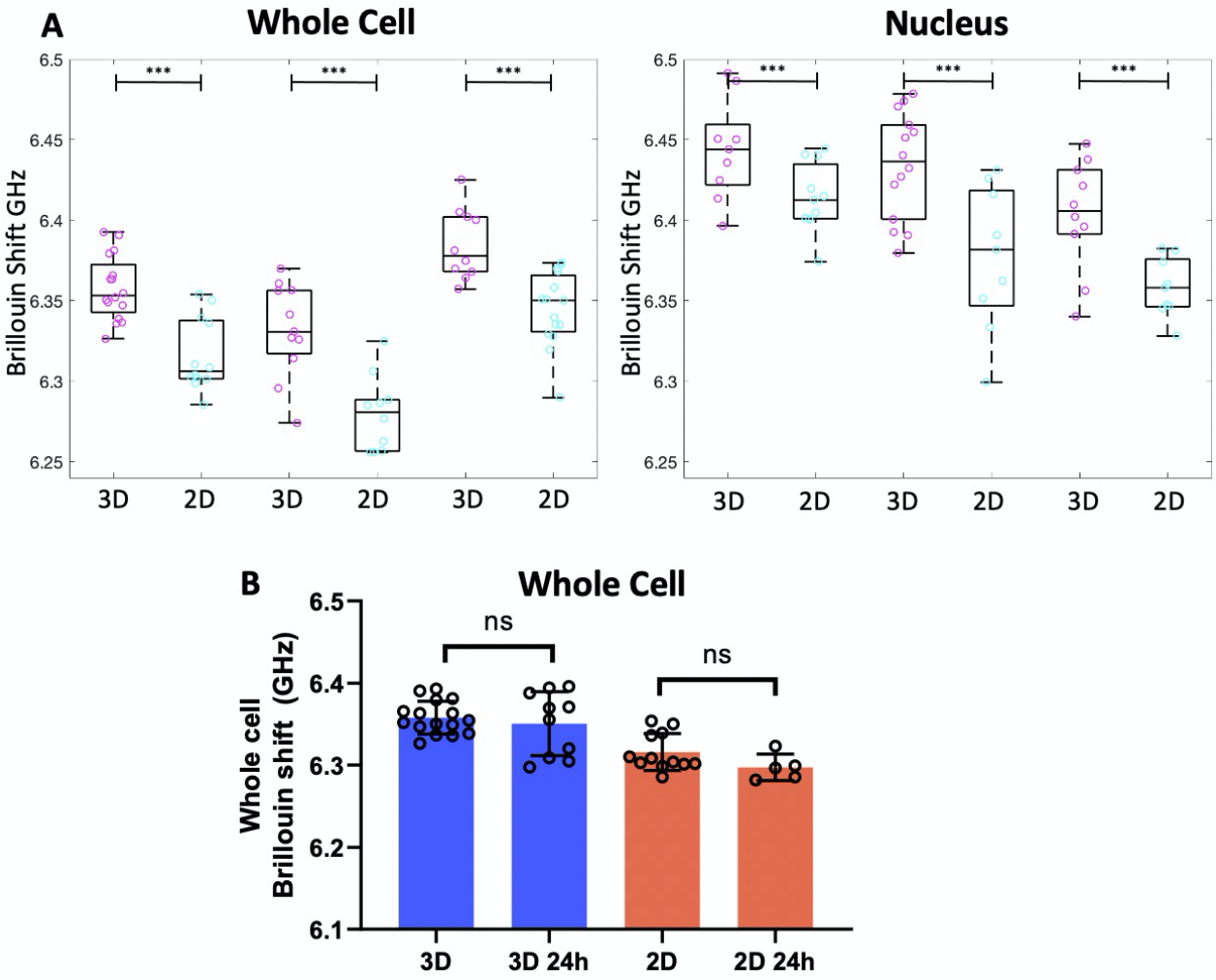

Figure S5: Brillouin Shift of the endothelial monolayer does not change during TEM. Brillouin shift of the endothelial monolayer before, during and after TEM. The mean Brillouin shifts for three conditions are 6.18 GHz (Before), 6.18 GHz. (2-sample t-test).